

Key Points:

- Of the identified and measured >2 million lunar craters, 1.3 million are ≥ 1 km in diameter
- Found more craters $\lesssim 30$ km than all other published catalogs, likely due to multiple data sets used and including subdued and secondary craters
- More elliptical craters are found than past work, orientation of $D \geq 10$ km craters are random, and many spatial density trends are discussed

Supporting Information:

- Supporting Information S1

Correspondence to:

S. J. Robbins,
stuart.robbins@colorado.edu

Citation:

Robbins, S. J. (2019). A new global database of lunar impact craters >1 – 2 km: 1. Crater locations and sizes, comparisons with published databases, and global analysis. *Journal of Geophysical Research: Planets*, 124, 871–892. <https://doi.org/10.1029/2018JE005592>

Received 28 FEB 2018

Accepted 21 NOV 2018

Accepted article online 26 NOV 2018

Published online 3 APR 2019

A New Global Database of Lunar Impact Craters >1 – 2 km: 1. Crater Locations and Sizes, Comparisons With Published Databases, and Global Analysis

Stuart J. Robbins¹ 

¹Southwest Research Institute, Boulder, CO, USA

Abstract This paper presents a new, global database of lunar impact craters, estimated to be a complete census of all craters with diameters larger than 1–2 km. The database contains over 2 million craters, making it larger in number than any previously published lunar effort by more than a factor of 10. Of those craters, 1.3 million have diameters ≥ 1 km, approximately 83,000 are ≥ 5 km, and 6,972 craters are ≥ 20 km. How the database was constructed along with the reliability of features is described in detail. Comparisons are made with past published databases, demonstrating good agreement for crater size and location. An ellipticity analysis is conducted, illustrating there is no dominant direction for elliptical crater orientation based on location, diameter range, or ellipticity amount, consistent with randomness for craters ≥ 10 km. A spatial density analysis is described, comparing the spatial density of small versus large craters, and numerous observations about the nonuniformity of the size distributions of craters across the Moon are made. The spatial density is also used in a discussion about kilometer-scale secondary impact craters and clearly shows that they dominate the crater population in some areas of the lunar surface. This paper presents just a tiny sample of the scientific investigations that could be done with this new crater database.

Plain Language Summary This work presents a new database of lunar impact craters. Over 2 million craters were identified and measured, and 1.3 million of them are larger than 1 km in diameter. The database is estimated to be a complete census of all craters larger than approximately 1 to 2 km across. Where there are overlaps, this database compares well with past databases with respect to crater diameters and locations, but the database contains more craters smaller than about 20 km across than any other crater database. This increase is attributed primarily to the fully manual effort involved in searching multiple instruments' data sets, using both imagery and topography, and multiple searches of the lunar surface. A spatial density analysis of the craters in different diameter ranges shows many trends that have been seen before, but it also reveals details of nonuniformity, which have not been previously described, including an enhanced small crater population at the Moon's north pole and many effects of secondary craters—craters that form from the ejecta of a larger, primary impact. Additionally, the database contains ellipse properties of the craters, and it shows that large craters' orientations are indistinguishable from randomness.

1. Introduction

Earth's moon has been observed for eons, and the impact craters that dominate its surface have been systematically recorded for centuries. Crater databases are useful for feature identification, landing site hazards, understanding impact physics, dating the relative ages of surfaces, and a myriad of other research investigations. The act of building a database itself is often a starting point for many planetary surface studies, and, for bodies where impact craters are the dominant landform (most known bodies in the solar system), a crater database is an important research endeavor. Public, published databases of these features can significantly speed other analyses because that first step has been completed. Therefore, planetary landform feature databases are still an important part of academic literature.

For the past several years, I have worked to build a large, global database of lunar impact craters. There are presently 2,033,574 craters in this database, and 1,296,879 of them have diameters $D \geq 1$ km. The database of $D \geq 1$ km craters is released via NASA's Planetary Data System's Cartography and Imaging Sciences Node Annex, available at https://astrogeology.usgs.gov/search/map/Moon/Research/Craters/RobbinsCraterDatabase_20180815; it will be updated periodically, so please contact the corresponding author to receive notice of updates, and/or for $D < 1$ km craters.

In this paper, the database is described in detail: Section 2 provides historic context. Section 3 describes how the database was constructed with important caveats on some parameters. Section 4 contains comparisons with previously published work. Section 5 describes several trends visible from this database (ellipticity analysis and observations from spatial density maps). Section 6 summarizes the work and future expansion. Appendix A contains a summary of all current database columns. Additional discussion of methods, auxiliary comparisons with prior work, supporting analyses, and additional figures are included in the supporting information.

2. Previous Lunar Crater Databases

Recording lunar impact craters can be traced at least informally to Galileo Galilei when he sketched craters from his telescopic observations and realized they were a topographic feature (Galilei, 1610). While nomenclature systems and basic feature cataloging were developed throughout the 1600s and later centuries (e.g., Riccioli, 1651), formal, internationally recognized cataloging did not begin for another three centuries. The first modern crater catalog is generally considered to be the work of Mary Blagg and Karl Müller who created the first official version of the International Astronomical Union's (IAU's) lunar features (Blagg et al., 1935). Their work was followed by Baldwin (1949) and Young (1953) who cataloged numerous lunar craters, and then a multiyear four-part catalog of ~17,000 craters published by D. W. G. Arthur and colleagues (Arthur et al., 1964; Arthur, Agnieray, Horvath, et al., 1965; Arthur, Agnieray, Pellicori, et al., 1965; Arthur et al., 1966) that attempted to identify all craters with diameters $D \geq 3.5$ km and some additional—though only named—smaller craters. A decade later, Wood and Andersson (1978) published a global catalog of ~11,500 named craters. A decade after that, Rodionova et al. (1987) published a catalog of 14,923 $D \geq 10$ km craters.

There was a lull in lunar crater cataloging that corresponded with the lull in NASA's lunar exploration, and the first large efforts with modern imagery and the next generation of spacecraft was Losiak et al. (2009), who updated what is colloquially known as "The LPI" lunar crater catalog. The LPI catalog was further revised by Öhman (2015) and currently numbers 8716 craters with $1 \lesssim D \lesssim 3,000$ km. It is far from a complete catalog at those diameters and instead focused on important and IAU-named craters.

The first modern global cataloging effort of craters larger than a certain diameter was Head et al. (2010) that released a $D \geq 20$ km database made with the first-generation digital terrain model (DTM) produced by the Lunar Reconnaissance Orbiter's (LRO's) Lunar Orbiter Laser Altimeter (LOLA). The database contains 5,185 craters. Subsequent work has demonstrated that it underreports craters $D \lesssim 30$ km (C. I. Fassett, personal communication, 2016; see section 4.3), likely because of the focus solely on using DTMs and that the DTMs were first generation. Povilaitis et al. (2018) extended that database with a $D = 5\text{--}20$ km supplement based on Lunar Reconnaissance Orbiter Camera (LROC) Wide-Angle Camera (WAC) 100-m/px global mosaics and 100-m/px WAC-derived DTM (supplemented by LOLA for $\pm(78\text{--}90)^\circ\text{N}$). This work excluded ghost and other buried craters (Povilaitis et al., 2018; M. S. Robinson, personal communication, March 23, 2016). It contains 22,746 craters, bringing the $D \geq 5$ km census of the two catalogs to 27,931 craters. In addition, at the time of this writing, Barlow and colleagues (Barlow et al., 2012) are completing efforts on a $D \geq 5$ km crater catalog that contains 30,123 craters $D \geq 5$ km that specifically excludes secondary craters (N. G. Barlow, personal communication, March 19, 2016), yet it has 8% more craters than the combined Head et al. (2010) + Povilaitis et al. (2018) catalogs (Barlow catalog crater number subject to change, for the above number is based on a preliminary presentation of their work).

Intermediate in publication date, two semiautomated or fully automated crater catalogs have been published. In this paper, "manual" means computer algorithms did not assist in crater identification and measurement, fully automated had no human interaction in crater identification and measurement, and semiautomated is intermediate, such as including human adjustment of automated craters. Salamunićcar et al. (2012, 2014) published lunar catalogs with 60,645 and 78,287 craters, respectively, based on automated detection in elevation data. The former was stated to be complete for craters $\gtrsim 8$ km. Wang et al. (2015) published an automated crater catalog of 106,016 craters made from *Chang'E-1* (嫦娥一号) images and DTM. The paper did not suggest a completeness limit other than ≥ 10 pixels, corresponding to $D > 1.2$ km, and it estimated a detection rate of 75.8%.

Cataloging lunar impacts has a long history, but it is only recently that researchers have been able to produce global catalogs, and even more recently that we have been able to produce global catalogs from a reasonably

consistent image base. While the catalogs vary in numbers of craters $D > 5$ km (27,931 for Head et al., 2010 with Povilaitis et al., 2018; 30,123 for Barlow, 2017; and 38,171 for Wang et al., 2015), and some of that variation will be due to inclusion or exclusion of secondary craters, they all have tens of thousands of craters of that diameter and larger. It is likely because of this large number that only automated efforts have so far been used on the Moon to compile larger catalogs to smaller crater diameters.

3. Generating a New Global Lunar Crater Database, and Information Contained Within

This section describes how craters were identified and measured, detail about the data sets used, what information is included for each crater, and important uncertainties and caveats. From this point, the database presented in this work will simply be called “the database,” and other databases will be referred to by their references.

3.1. Assumptions

The assumption used in this work to identify lunar impact craters is that, on the Moon, the vast majority of quasi-circular depression features are impact craters, and that elongated quasi-ellipsoidal features with the long axis radial to a much larger crater are impact-caused features. This assumption can be violated by geologic context, such as valleys between mountains, pit craters, or landslides with circular termini that encircle a depression (e.g., perhaps caused by a small crater impacting a larger crater’s rim or wall). The assumption will not have universal application because a variety of geologic processes can cause circular depressions, but most of those do not occur, or occur with relatively low frequency, on the Moon. An additional decision was that if a crater appeared to be fairly elliptical, and it appeared as though there was a cusp on both sides of the crater rim roughly in the middle of the long axis, it was cataloged as two separate craters rather than one highly elliptical crater.

3.2. Crater Identification Method

Crater rims were manually identified in *ArcMap* software in approximately local coordinates: Equidistant cylindrical for $\lesssim |\pm 35^\circ|$ latitude, Molleweide with a local prime meridian for $\approx \pm(35\text{--}60^\circ)$ latitude, and polar stereographic for $> |\pm 60^\circ|$ latitude, though all projection effects were removed in later steps. Crater rims were manually traced using the “streaming” function to create a vertex every N meters. The vertex spacing was set to $2.5 \times$ the image pixel scale. However, when ESRI released *ArcMap* 10.0, streaming became tied to screen resolution and when maps were displayed full screen, computers available at the time this work began could not keep up with that vertex spacing when drawing at a reasonable pace. Therefore, the true vertex spacing is sparser: A best-fit line to the database (with significant scatter, especially at small diameters) is $N = 8.1 + 4.1 \cdot D$ where D is in kilometers; the minimum is 6 points (5 are required to uniquely define an ellipse, 3 to define a circle), the maximum is 8,088 (Orientale), and ~ 31 million points were used in total. For a $D = 1$ km crater, this translates to roughly 12 points to define a crater rim in the main image data used, which is significantly more than the usual standard in the crater measurement field (typically a 2-point cord defines a diameter or 3-point method defines a circle; Robbins et al., 2014). Tracing was done over a large range of scales; the most common was 1:100,000, though coarser scales were used for larger craters and finer scales for higher-resolution data sets.

3.3. Data Used for Crater Mapping

The database was generated through a fully manual effort using data from the following instruments: LRO Camera’s (LROC) WAC (Robinson et al., 2010), LRO’s LOLA (Smith et al., 2009), and Terrain Camera (TC) on SELENE or “Kaguya” (かぐや; Haruyama et al., 2012).

First, craters were identified and traced using the WAC “morphologic” mosaic, created by the LROC team by mosaicking monochrome (643 nm) WAC images with an average 58° sun angle from vertical. These were supplemented with “dawn” and “dusk” mosaics that have the sun closer to the horizon, which makes mapping topographic features like craters easier but which masks smaller craters that are in deep shadows. The dawn and dusk maps were not used initially because they are poorly controlled with multikilometer offsets in some areas as of the version released in mid-2015. All public WAC mosaics were 100-m/px. Additionally, I produced several custom, more local WAC mosaics closer to the native ≈ 70 -m/px using a variety of narrow-range solar incidence angles, generally $> 70^\circ$ sun. These custom mosaics were useful in areas where, for

example, the morphologic mosaic's sun angle was too high to easily identify craters, but the dawn or dusk mosaics' sun angle was too low to identify craters in the shadow of other large topographic features. These custom mosaics were produced using SPICE data from USGS throughout 2017 and visibly appeared to be within a few pixels (hundreds of meters) of the WAC morphologic mosaic. Toward the lunar poles, the sun angle increases significantly in all image-based products, but for consistency with the equatorial regions, the WAC mosaics were still used for the initial crater identification. The entire Moon was searched twice using WAC mosaics.

Second, LOLA gridded data record (LOLA GDR), and a merged TC DTM and LOLA mosaic (Barker et al., 2016), were used. The former is available globally, and the latter is available within $\pm 60^\circ$ of the equator. Both are 512 pixels per degree, which corresponds to $\approx 59\text{-m}/\text{px}$ at the equator, and there were no visible offsets from the WAC global product in either topography data set. In general, the merged TC DTM + LOLA mosaic was used where it was available: Despite the success of the LOLA instrument and return of >6.8 billion valid data points as of the time of this writing (Smith et al., 2017), there are still multikilometer-wide gaps in the LOLA data set at the lunar equator. The opposite is true at both poles, for LRO is in a polar orbit, and so the poles have a much higher spatial density of data points. Therefore, LOLA GDR are currently available at up to 5-m/px within 2.5° of both poles. For regions near the poles, hillshade maps were produced from the LOLA GDR using *ArcToolbox*'s hillshade utility, and it was mostly on the hillshade that craters were identified and measured. This was often supplemented with the elevation data overlaid. As with WAC, two searches across the Moon were made using only topography to search for additional impact craters. During this effort, if craters appeared to have been poorly traced in the image data, they were removed and re-done in topography. "Poorly traced" here was most often when higher sun in the WAC mosaics made distinguishing a crater rim more difficult and erroneous in places, and it was more distinct in topography data.

Finally, in some regions for related lunar crater work, TC mosaics at 30-m/px were used to identify impact craters. At the time of this writing, the TC effort has almost exclusively been undertaken in some lunar maria. As with the initial topography-based search, if a crater appeared to be previously poorly defined relative to the TC mosaics, they were removed and retraced. Due to occasional positional inaccuracies with the TC mosaics, if there were offsets, the crater traces were moved to their approximate positions in a lower resolution data set.

The last step was to compare the large crater results with those from the GRAIL crater database (Neumann et al., 2015). That work has 74 features $D \geq 200$ km, and all but 15 of them exist in this database. The 15 not in this database are because there was no clear topographic signature, and all 15 were "proposed" in Neumann et al. (2015). Additionally, craters in this database were revised if the diameters differed by $>10\%$. All but two craters that were revised, Imbrium and "TOPO-13," now differ by $<10\%$ (in this work, Imbrium is smaller by 10.3%, and TOPO-13 is larger by 23.3%). Finally, there are two features $D \geq 200$ km in this database not in the GRAIL database: Tranquillitatis and Janssen. Tranquillitatis appears to be a crater so it is retained in this database, and Janssen is fit as $D = 203$ km so a slightly smaller diameter from GRAIL likely accounts for that omission.

3.4. Circle Fitting

Vertices were recorded as latitude and longitude in units of decimal degrees, and data were output from the GIS (geographic information system) shapefile format and read into *Igor Pro* software. Custom code developed and validated over the past decade (e.g., Robbins & Hynek, 2012) took each crater rim's vertices and projected them into kilometers from the centroid of the points. This projection used Great Circle distances and bearings (Vincenty, 1975) to account for projection effects (validated by returning meaningful fits for Shackleton crater that contains the lunar south pole). The code then fit a circle via a custom nonlinear least-squares iterative Gauss-Newton routine, recording the crater's center (decimal degrees) and diameter (kilometers). Uncertainty in the crater diameter was recorded as the standard deviation of all vertex points' distance from the crater center minus the fitted crater radius (see section 3.6 for why this is a minimum measure of uncertainty). A second fit was done using a singular-value decomposition implementation of the Taubin (1991) implicit fit, considered by some to be the best algebraic circle fit (Al-Sharadqah & Chernov, 2009). The fit that returned a diameter closer to the mean of the ellipse fit axes and had a smaller residual in the rim points (the recorded diameter uncertainty) is what was saved.

3.5. Ellipse Fitting and Parameter Robustness

The code fit an ellipse to the points using the approximate maximum-likelihood (AML) method of Szpak et al. (2015). Crater center (decimal degrees), major (a) and minor (b) axes (kilometers), tilt angle (0° to 180° , counterclockwise for the major axis, where 0° means the major axis is in an East-West direction), ellipticity $e = a/b$, and eccentricity $\epsilon = (1 - b^2/a^2)^{1/2}$ were recorded along with standard errors for each value. Through extensive testing, the newer AML method was found to be significantly more robust than the direct (DIR) method of Fitzgibbon et al. (1999) used by many other researchers. However, as an iterative method without parameter constraints, poor fits could sometimes result. Therefore, if the fitted ellipticity is >4 , the fitted ellipticity parameters were rejected for that crater (52 of 2,033,574 craters). While this could reject some valid fits for extremely elongated secondary craters, I think it is better to remove more false fits. The end user of the database can impose a more stringent cutoff if desired.

Since publication of the Mars database (Robbins & Hynek, 2012), significant questions have arisen about these parameters, so brief discussion in this main text is warranted: First, there was a bug where tilt angle may be flipped by $\pm 90^\circ$; this has been fixed. Second, tilt angle spanned -45° to $+135^\circ$, and that has been changed to 0 – 180° . Third, extensive analysis and Monte Carlo simulations in that paper demonstrated there was a strong bias for small craters to have an elliptical solution even if they are perfectly circular and that still holds in this database. Fourth, there was a bias in the tilt angle direction that also exists in this database, though at a smaller maximum diameter (see the supporting information). The data still have utility so are supplied in this database, but the warning remains and is elaborated on in section 5.1 and the supporting information: Craters with $D \lesssim 10$ km and especially those with $e \lesssim 1.25$ should have their ellipse properties treated with caution (see the supporting information for more on this cutoff and additional, supporting figures). Finally, a basic quality check was undertaken and craters were reexamined if (1) they were in the ~ 99.5 th percentile of ellipticities for craters within $\pm 1\% \cdot D$, and/or (2) their diameters satisfied the condition $D < 1.1^{-1} \cdot D_{\text{minor}}$ or $1.1 \cdot D_{\text{major}} < D$. The latter criterion was met most often when $\ll 50\%$ of the rim could be traced, though this was rarer when using the AML fit method instead of DIR (see the supporting information for further discussion).

An additional parameter was calculated that estimates the fraction of the crater rim that was traced. Because vertex points were not placed at every pixel, the algorithm operates by calculating the bearing from the crater center to each rim point, sorting the rim points based on bearing, and calculating the distance from one rim point to the next in the sorted list. The median distance is calculated, and any gap in distance $>2 \times$ the median is considered as not traced (this $2 \times$ value is somewhat arbitrary). The bearing start and end of the gaps is measured, multiple gap spans are summed, and that sum is subtracted from 360° . The result is divided by 360° and recorded. The intent of this column is to provide an additional guide for whether recorded values are reliable: If there was little of the arc traced, then ellipse and circle fits may be prone to more uncertainty beyond the formal errors given. This is only a guide, however, for some very large craters were marked by very few points. For example, in the current database, Nubium, $D \approx 660$ km, was marked with only 15 points, but because those points were almost equidistant, this algorithm reports the arc completeness as 81%. For the majority of the database, however, it should provide a reasonable metric in addition to the formal uncertainties about how reliable the ellipse fit is.

3.6. Intracatalog Errors and Uncertainties in Crater Measurements

Various sources of error (difference between a measured and true value) and uncertainty (dispersion of values attributed to a measured quantity) are described in this section. There are four sources of error and uncertainty in constructing this catalog: Data, human, projection, and parameterization of a complicated geometric shape.

3.6.1. Data

These arise from errors in projection from the image plane to a map base and from the finite scales of pixels. The lunar coordinate system is currently very well defined based on LOLA data. However, some products are not well controlled (dawn and dusk WAC mosaics and TC mosaics), which can result in positional errors of roughly hundreds of meters relative to the current lunar control network. This also affects older data sets or those with poor control, such that in the next section comparing this database with others, existing offsets may not be due to errors in this database, but errors in other lunar control networks.

3.6.2. Human Identification

Human-based errors and uncertainties dominate over other sources. In crater detection, this involves the ability to identify a crater and the subjectivity of whether an individual considers a feature to be an impact crater. This interresearcher variability was examined most recently by Robbins et al. (2014), and they found a 1σ variation in number of craters identified by eight different researchers to be as low as $\pm 15\%$ (lunar maria) and as high as $\pm 40\%$ (lunar highlands). Much of the variation stems from different philosophies with respect to feature cataloging: Should a feature that might be a crater be included in the database? Some researchers are conservative and include only features the researcher is certain or almost certain are impact craters. Some researchers are liberal and include features the researcher thinks have a lower possibility of being impact craters. In modern cataloging, the Povilaitis et al. (2018) work followed the conservative approach, but the work on this database follows the liberal approach. This approach is especially manifest around Orientale crater, where large, nearly circular depressions that are included in this database as impact craters are not in many other databases.

3.6.3. Human Measurement

Humans are not unbiased algorithms, and where one measures the rim is subject to human bias and bias based on data quality and data type (e.g., an idealized crater will have zero shading for the rim points parallel to the light source, making that portion of rim identification difficult). While sharp, well-defined rims are often prone to diameter uncertainty $\sim \pm 5\%$, more subdued rims can have diameter uncertainty $\sim \pm 10\%$ (Robbins et al., 2014).

3.6.4. Projection

This refers to the projection from decimal degrees to an absolute length unit for circle fitting and ellipse fitting. While using Great Circle distances and bearings is likely the most accurate projection method that exists with stated errors of fractions of a millimeter (Vincenty, 1975), it still has assumptions involved, and simplifying assumptions were used in this work. The largest assumption is that the Moon is a sphere with radius 1,737.1513 km, but it is better represented as a biaxial ellipse with a polar radius 1,735.6576 km and equatorial radius 1,737.8981 km (Smith et al., 2017). It also has topographic variation on the scale of $\sim \pm 8\text{--}9$ km (Smith et al., 2017) such that the local radius at any given point could vary by several kilometers from the mean radius used. Using a different radius scales crater diameters by that radius, such that ± 10 km adds a maximum $\pm 1\%$ to diameter measurements. This is negligible relative to other sources of error and uncertainty so is not factored into the database. However, it is included here because it is a source of error and will be especially important on small bodies.

3.6.5. Parameterization

Craters are not ideal, simple geometric features, and parameterization by circle fitting and ellipse fitting introduces errors and uncertainty based on deviations from that ideal. Formal derivations exist for calculating the error on each fit parameter, but whether those are useful in understanding crater data is debatable. Instead, this database includes one metric of error + uncertainty based on variation of the digitized rim from the circle fit: Distances between each vertex point and the fitted crater center are subtracted from the fitted radius, and the standard deviation of those residuals is calculated and saved. The uncertainty approximately follows a power law with significant scatter for $D \lesssim 5$ km: $\delta D = \gamma + \beta \cdot D^\alpha$ for $D \in (0.1, 2500)$, where $\gamma = 0.016 \pm 0.022$, $\beta = 0.020 \pm 0.003$, and $\alpha = 0.99 \pm 0.03$, via a least-squares regression. A more robust fit (York et al., 2004) with a fixed $\gamma = 0$ has $\beta = 0.024 \pm 0.000$ and $\alpha = 1.17 \pm 0.01$. The fit holds over 5 orders of magnitude. Because the rims were manually identified on images and DTMs, inherent within this parameter is random error from both the data-based errors and human-based uncertainty and errors. While I am exploring methods to minimize the small, generally few pixel deviations inherent to manual rim identification, that work will be in a future report and it is not possible to separate from the parameterization at this time. Additionally, formal uncertainties are included for every ellipse parameter.

3.6.6. Summary

There are numerous sources of error and uncertainty in building even a relatively basic features catalog. Keeping those in mind is imperative in reasonable use and applications of the database. In this work, measured uncertainties in diameters (due to parameterization of a nonideal shape) are between order $\pm 1\%$ and $\pm 10\%$, and additional uncertainties based on human interpretation of features are likely larger, but they are not characterized in this database. However, in the next section, they are examined empirically based on a comparison with other data bases.

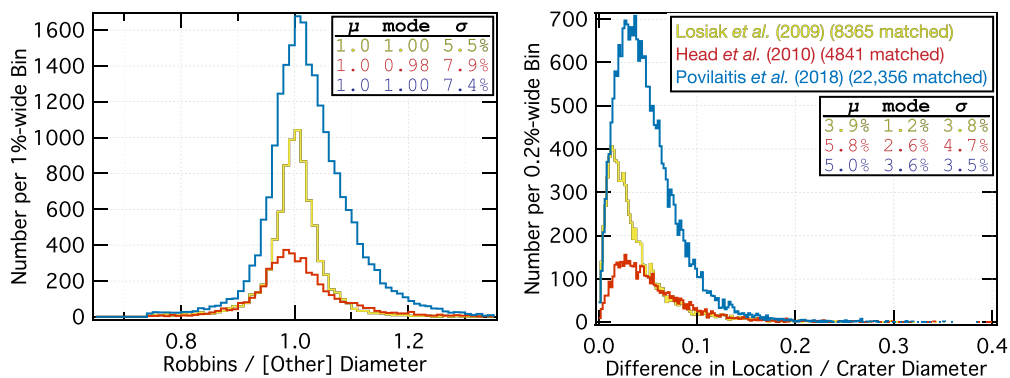


Figure 1. Histogram of matched craters between three published crater databases and this database; color is the same in both panels. (left) Values >1.0 on the horizontal axis indicate craters are larger in this database, and <1.0 indicates craters are larger in the other catalog. (right) Values are the difference in location of the crater center in each catalog versus this database, divided by the crater diameter in this database. The legend indicates number of craters matched from each catalog to this database, and the extra legends indicate the mean, mode, and standard deviation (assuming a Gaussian distribution) for each matched comparison.

4. Comparison With Existing Global Lunar Crater Databases: Location, Diameter, and Discussion of Completeness

This section describes this database in comparison with currently public lunar crater databases. Based on that comparison, I provide an assessment of the “completeness” of the database both locally and as a whole. In the first two subsections comparing locations and diameters, data are compared with the three manual catalogs described in section 2: Losiak et al. (2009) revised by Öhman (2015), Head et al. (2010), and Povilaitis et al. (2018). In the first two subsections, craters were matched between databases via a clustering algorithm (Ester et al., 1996; implementation for craters by Robbins et al., 2014) where the matching criteria between craters in each database required (1) distance $\leq 0.375 \cdot \text{avg}(D_1 + D_2)$, and (2) diameter ratio ($|D_1 - D_2| \leq 0.375 \cdot \min(D_1, D_2)$). Comparison with the LPI catalog ignores some features because of errors in that catalog due to its reliance on the IAU’s nomenclature and features. For example, “crater” Van de Graaff is recognized by the IAU to be a single feature at -27.0°N , 172.0°E , $D = 240.5$ km, which is how it is listed in the LPI catalog. However, both Head et al. (2010) and this database recognize it is clearly two distinct craters, in this database at -26.1°N , 173.4°E , $D = 140$ km, and -28.2°N , 170.6°E , $D = 147$ km. Additionally, all catalogs had large variations in how they defined many of the largest lunar craters—in some cases by factors of $>50\%$ —so for this database the large craters were checked against the GRAIL large crater database and revised if there were offsets (see section 3.3).

4.1. Diameter Comparisons

The left panel in Figure 1 illustrates histograms of the ratio of matched craters’ diameters to those in this catalog. These data demonstrate there is no significant bias for any catalog to report larger or smaller crater diameters. The diameters generally agree to within $\pm 5.5\text{--}7.9\%$ (1σ), which is in agreement with—if slightly smaller than—the experiment in Robbins et al. (2014), which may have been a worst-case situation of replicability. This result was independent of crater diameter (see the supporting information).

4.2. Location Comparisons

The right panel in Figure 1 illustrates histograms of the ratio of matched craters’ locations relative to their diameter. These data demonstrate that craters are generally within $<4\%$ of a crater diameter from each other, and $>90\%$ of the craters are within $\sim 10\%$, also a similar result to the data in Robbins et al. (2014). This result had a small dependence on diameter, where smaller diameter craters had centers that were farther apart relative to their diameters (see the supporting information) and could be due to an evolving lunar coordinate system.

4.3. Completeness Comparisons

A different kind of comparison can be made with other databases to compare completeness, shown in Figure 2. This comparison shows a SFD_{EDF} based on the recommendations of Robbins et al. (2018),

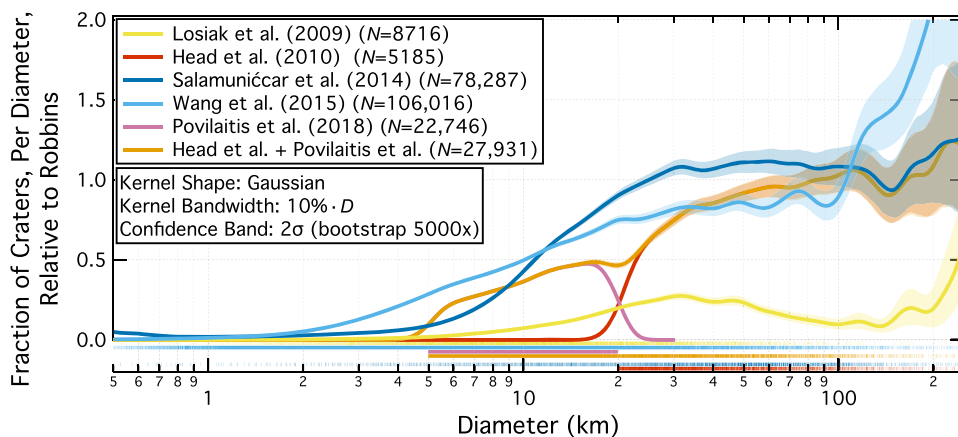


Figure 2. SFD_{EDF} for several data sets relative to the database in this paper; values >1 are where those databases have more craters, and <1 are where this database has more craters. The diameter range is limited to $D = 0.5\text{--}250\text{ km}$ to emphasize where most databases overlap; $D > 250\text{ km}$ has so few craters that the confidence bands all overlap and are not shown. Automated databases are blue, the LPI catalog is yellow, and the databases meant to be used together are pink and red, and combined as orange. The rug plot at the bottom indicates each original crater diameter. See section 4.3 for discussion.

which instead of binning craters in discrete diameter bins, treats each crater as a Gaussian distribution with a mean at the measured diameter and standard deviation $10\% \cdot D$ (based on the Robbins et al., 2014, study). This process is known as an empirical distribution function, and to distinguish the resulting size-frequency distribution (SFD) from the classic binned method, a subscript “EDF” is used. After the incremental SFD_{EDF} (ISFD_{EDF}) was built for each database, each was divided by this database’s ISFD_{EDF}, creating a relative version (not the same as a relative SFD, or “R-plot”). A caveat in interpreting the SFD_{EDF} is there will be an artificial decrease near the completeness limit of any data set, and this decrease is magnified when the cutoff is abrupt (i.e., a truncated data set). It is visible within $\approx 2\text{--}3\sigma$ of the limiting diameter, so when using $\sigma = 10\% \cdot D$ for Head et al. (2010), this decrease only affects craters $\lesssim 25\text{ km}$. For that reason, the Head et al. (2010) and Povilaitis et al. (2018) data sets are included as a merged data set in Figure 2, such that this technique introduces no artifact near the merged diameters (i.e., the $D \approx 20\text{ km}$ deviation is real). The rest of this section describes observations based on this Figure; for additional comparisons using spatial density, see the supporting information.

First, the manual data set of Head et al. (2010) shows good agreement with this work for craters $D \gtrsim 50\text{ km}$. For $D \approx 35\text{--}50\text{ km}$, there is a deficit in that data set that increases as diameter decreases, to about 10% fewer than the number in this database; for $D = 20$ to $\approx 35\text{ km}$, the decrease is significantly more, down by as much as $\approx 50\%$ near $\approx 20\text{ km}$. This decrease makes sense when one considers the early LOLA data product used and absence of image data in crater detection.

Second, the Povilaitis et al. (2018) data set continues the decrease in crater number relative to this catalog, starting at approximately 50% of the craters found (for $D \approx 20\text{ km}$) and dropping to $\sim 25\%$ (for $D \approx 5\text{ km}$). Given the caveat about the EDF artifact for $D \approx 5\text{--}7$ and $16\text{--}20\text{ km}$ craters, one can also examine the merged data sets and see that there is a mismatch near $D = 20\text{ km}$, where the two data sets are supposed to line up. That analysis shows the divot is a real feature, not an artifact of the SFD_{EDF}, where the researchers did not identify all 20 km and those slightly smaller than it. Even if this new database is overcounting craters, it is very unlikely that I significantly overcounted craters just at diameters near 20 km.

Third, the Salamunićcar et al. (2014) data set, an improvement over Salamunićcar et al. (2012), is shown to have more craters relative to this data set (and Head et al., 2010) for craters $D \gtrsim 30\text{ km}$. For $D \lesssim 30\text{ km}$, a similar drop in number of craters relative to this catalog as diameter decreases is observed, such that fewer $D \approx 8\text{ km}$ craters were found than identified by Povilaitis et al. (2018).

Fourth, Wang et al. (2015) has $>2\times$ more craters $D \gtrsim 100\text{ km}$ than any other researcher (and 30% more $D \geq 200\text{ km}$ than the GRAIL-based catalog), but they are near or slightly below parity relative to this

catalog and the Head et al. (2010) work for $D \approx 30\text{--}100\text{ km}$ craters. For $D \lesssim 30\text{ km}$, the relative fraction again drops with decreasing diameter, though less quickly than the Salamunićcar et al. (2014) data. They consistently found more craters than Povilaitis et al. (2018) by roughly 30% (or by 10% relative to this paper's database). It should be noted that a more detailed analysis of the Wang et al. (2015) catalog indicates they omitted a cosine(latitude) scaling to crater diameters required as a result of map projection, which, if it had been properly applied, would produce a database more consistent with (though still with significant offsets from) other databases.

In summary, the databases generally agree on crater numbers for craters $D \gtrsim 30\text{ km}$, but for smaller diameters, there is significant disagreement, especially relative to this database. There are a few *a priori* reasons why this might be. This database includes ghost, heavily degraded, and secondary craters, which are often hard to detect with automated codes. This database used both imagery from two different spacecraft and independent laser altimetry, while no other database has used both. Also, I have a lower threshold for what may be considered an impact crater than some other researchers. However, a relative SFD of this database is flat for $\sim 2\text{--}20\text{-km}$ craters, in agreement with other past work (e.g., Strom et al., 2015, and references therein), in contrast with the other databases. So the reader has a more direct comparison to investigate this discrepancy, four roughly uniformly spaced locations across the Moon are in Figure 3, shown in topography and image data, and idealized circles for $D \geq 5\text{ km}$ craters from this catalog (blue) and Head et al. (2010; dark red) with Povilaitis et al. (2018; light red) are overlaid.

4.4. Additional Completeness Discussion: Completeness Based on This Database Alone

Several currently existing databases state a completeness estimate, which is the minimum diameter that is estimated to contain a complete sample of all existing craters (this can be a conscious choice by the researcher or based on limiting resolution of the data). Head et al. (2010) tried to ensure completeness by overlaying a 20-km reference grid and including features larger than the grid. Povilaitis et al. (2018) do not state how they determined a complete $D = 5\text{--}20\text{ km}$ crater census, and they did not add any craters $D \geq 20\text{ km}$. Salamunićcar et al. (2012) estimated $\gtrsim 8\text{ km}$ completeness based on a change in slope in a cumulative crater SFD.

For completeness estimation, the method I favor is an SFD analysis. This simple process is to calculate an ISFD, determine where the derivative of the slope is zero, and some N th diameter bin larger than that is the completeness diameter. In Robbins and Hynek (2012), completeness was estimated to be one diameter bin larger than the diameter bin with the most craters (e.g., if using $2^{1/2}\cdot D$ multiplicative bins, and the diameter bin with a minimum diameter of 0.707 km has the largest number of craters, then the bin with a minimum of 1 km is considered to be the completeness limit; that and this work use $2^{1/8}\cdot D$ bins).

This metric has two fundamental assumptions, and violating either would render it inaccurate: (1) The crater population must continue to increase in number from large to small diameters through that completeness limit, and (2) when approaching that completeness limit, the researcher must identify 100% of existing craters until that limit is reached. For the Moon, assumption 1 is broadly true based on decades of research (e.g., Hartmann, 1965, 1999; Neukum, 1983; Neukum et al., 1975, 2001; Shoemaker et al., 1970), but there can be localized violations, such as recent resurfacing by a large impact crater and its ejecta (including large secondary craters). Assumption 2 was studied in a limited manner in Robbins et al. (2014) with varied results: Some researchers maintained a constant SFD slope until within ~ 1 bin of their estimated completeness limit, others' slopes increased, and others' slopes decreased. From these mixed results, it is difficult if not impossible to place a true value on the completeness limit of this database without an independent database that is "complete" to a significantly smaller diameter. However, none exists.

With those two assumptions made, the same basic procedure from Robbins and Hynek (2012) was followed here, but with one critical difference: Instead of a global result and instead of finite latitude \times longitude bins, a map was produced (Figure 4) using the above completeness criterion. For this map, a grid resolution of $0.5^\circ \times 0.5^\circ$ was used, where craters within a 151.5-km radius (equivalent to 5° at the equator) of any given point on the map were binned into an ISFD using $2^{1/8}\cdot D$ binning (for more details on how this and other maps were constructed, see the supporting information). From this map, lunar maria are mostly complete for craters $D \gtrsim 1\text{ km}$, the lunar poles where 5–10-m/px LOLA DTMs were used are also complete for $D \gtrsim 1\text{ km}$, but the lunar highlands tend toward completeness of only 1.0–1.5 km.

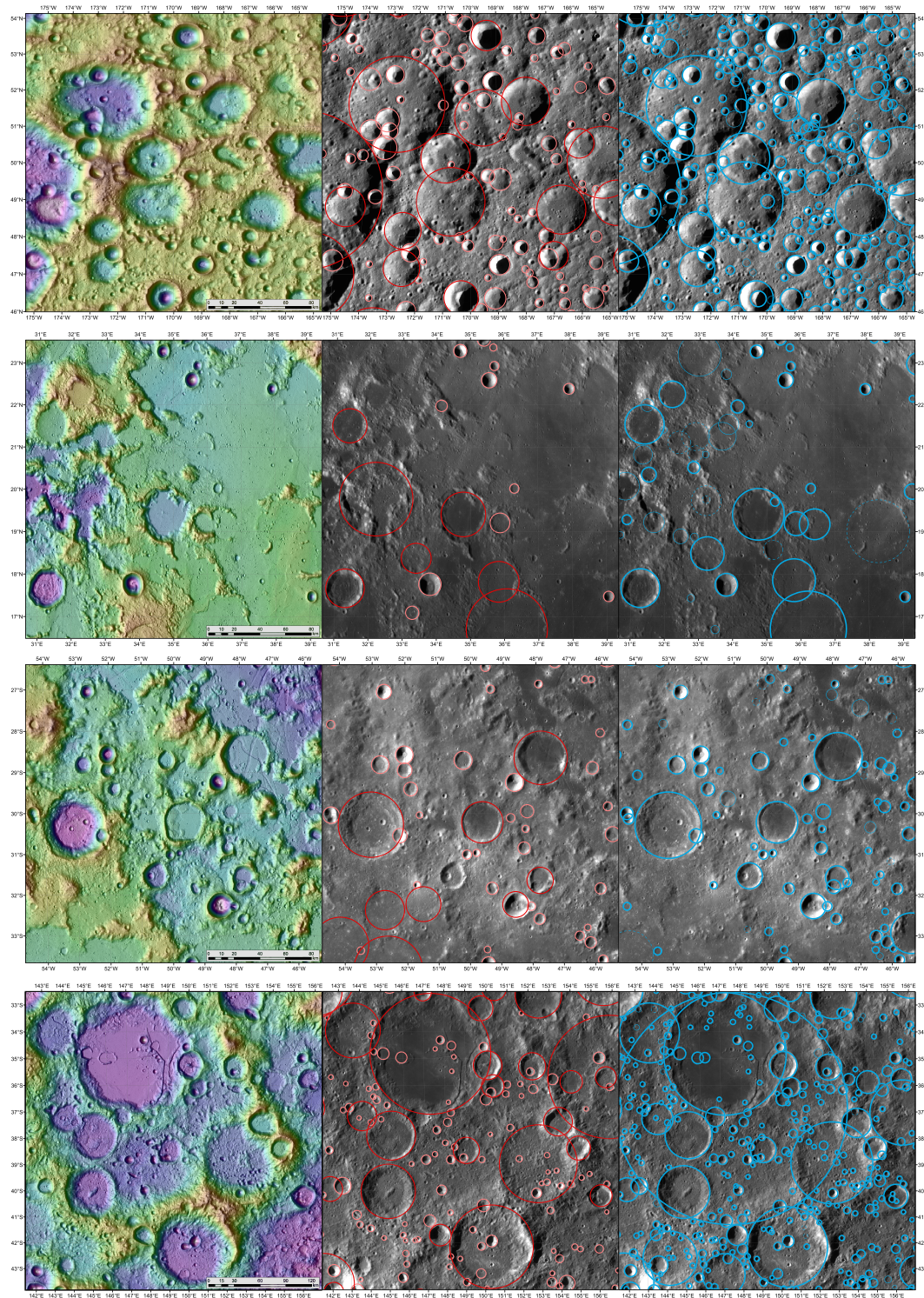


Figure 3. Several locations on the Moon (left) with idealized circles overlaid from the Head et al. (2010; middle, red) with Povilaitis et al. (2018; middle, pink) and this catalog (right, blue). For this catalog, preliminary confidence assignments have been made (see section 6) where thick circles are “certain,” thin are “likely,” and thin dashed are “possible.” Basemap on the right is TC DTM + LOLA shaded relief and color, basemap in the middle and on the left is WAC morphologic. Map projection is Mollweide with central longitudes in the middle of each row. All map scales are the same except the bottom row, which shows a larger region. Note on the smallest craters: There are some obvious small craters shown in one catalog and not the other, and the missing crater is likely due to small measurement difference and the strict $D \geq 5$ km cutoff.

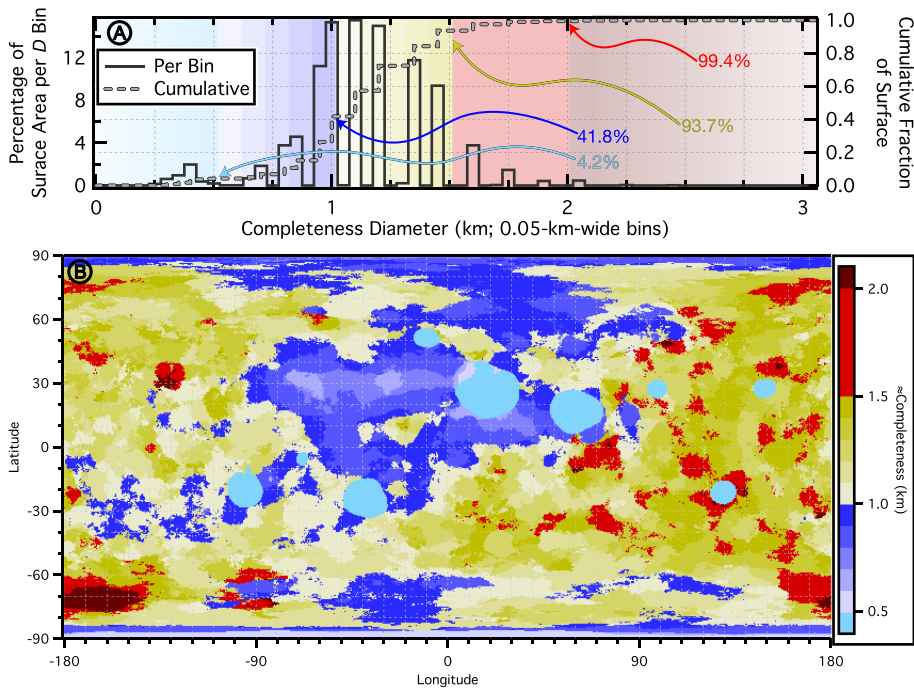


Figure 4. Completeness histogram and map of this crater database, based on the criterion and system explained in section 4.4. (a) Histogram of the completeness diameters, based on the map in panel (b), and color from panel (b) is faded in the background. The solid line is the percentage of the surface complete to that diameter (and larger) and uses the left vertical scale; the lighter dashed line is the cumulative fraction and uses the right vertical scale and grid. Arrows with percentages are cumulative percentage of the surface complete to that diameter crater or smaller. (b) Completeness map for craters within 151.5 km of each point on the map. Craters at each point were binned in $2^{1/8} \cdot D$ intervals into an ISFD, and the bin one-larger than the bin with the most craters, when searching from small to large craters, is stored as the completeness diameter. See the supporting information for more details and additional maps and methods.

From the map and histogram, 41.8% of the body is complete for $D \geq 1 \text{ km}$, 93.7% for $D \geq 1.5 \text{ km}$, and only four larger areas (and some smaller) covering 0.6% of the surface are worse than 2 km using this criterion: (1) Near the young lunar crater Kovalevskaya (30.9°N , -129.4°E); (2) in the region of the large Harkhebi crater ($D \approx 267 \text{ km}$) in which the younger Fabry crater is emplaced (43.1°N , 100.7°E), which is also near the young Giordano Bruno crater; (3) within ~ 1 crater diameter of the rim of Tsiolkovskiy crater (-19.9°N , 129.0°E); and (4) within ~ 2 crater diameters of Antoniadi crater (-69.4°N , 187.0°E). In these exceptions, it is likely that failure to identify sufficient craters $D \approx 3/4$ –2 km could be due to a real absence of craters rather than a failure to detect them. A plausible scenario is the surface was reset by the recent large crater(s), it was scoured with large secondaries and other ejecta (see discussion in section 5.2), and there has not yet been enough time to accumulate sufficient numbers of $\sim 1 \text{ km}$ craters to satisfy this completeness criterion.

Additionally, it is possible that much of the lunar highlands which are complete to $D \sim 1.0$ – 1.5 km are such because there is a real deficit of craters $D \sim 1.0 \text{ km}$. To test this, a $10^\circ \times 10^\circ$ region centered at 0°N 180°E was examined with *SELENE* TC mosaics with the goal to bring completeness to $D \sim 0.5$ – 0.8 km . Instead, while the completeness diameter decreased slightly, that region is still only complete to $D \sim 1.0$ – 1.2 km . This could be a real phenomenon for at least two nonmutually exclusive reasons. First, $D \sim 1 \text{ km}$ craters could be in saturation equilibrium in lunar highlands, partially as a result of diffusive erasure (e.g., implied by Fassett and Thomson (2014); inferred by Robbins et al. (2014)). This is supported by a limited (but not shown) saturation analysis which suggests that this region is saturated for craters $D \lesssim 7 \text{ km}$. Second, extreme topographic slopes in the lunar highlands not only make it difficult to form craters, but the erosion rates from meteorites and topographic diffusion are increased, also potentially rendering a true deficit of $D \sim 1 \text{ km}$ craters.

However, it is still possible that $D \sim 1 \text{ km}$ craters were missed, and the completeness map will necessarily shift to larger diameters if the SFD technique were modified to move more diameter bins from the peak. If the completeness criterion is made more conservative and it is $2^{1/2}$ rather than one $2^{1/8}$ bin greater than

the peak that is used, then the percentages shift such that 10.1% of the surface is complete for ≥ 1 km, but 93.8% is still complete for ≥ 2 km. For those reasons, the title of this paper emphasizes a conservative completeness to 1–2 km, not ≥ 1 km.

5. Database Properties and Implications

The purpose of this section is to examine this new database in two different ways that are uniquely available to it because of either the data contained (ellipse fits) or the small minimum diameter. This section is not meant to follow a standard scientific investigation of each topic, but rather to focus on background, observations, comparison with past work that has addressed the issue and develop hypotheses to potentially explain any differences observed. It does not test and then revise those hypotheses, for that is left to future work. The singular exception is the last set of observations about ellipticity where the ellipse tilt angle is tested for randomness.

5.1. Ellipticity Analysis

Ellipticity studies of lunar craters have been done before, and while many have focused on analyzing a subset of craters that are “obviously” elliptical, a few examined all craters within a given population, terrain, or on a given body (e.g., Bottke et al., 2000; Herrick et al., 2012). Those studies examined morphologically well preserved impacts. In reality, almost no craters are perfect circles, and this database’s construction method allows an unbiased analysis of any trends in crater ellipticity across the entire lunar surface. It is different from other work in that *all* impacts are examined as opposed to just those that are morphologically well preserved. Based on the uncertainty discussion in section 3.6 and the supporting information, only craters with $D \geq 10$ km and $e \geq 1.25$ are included in this analysis.

Bottke et al. (2000) is the most commonly cited study on lunar crater ellipticity. They studied 932 lunar craters, $D = 2.3\text{--}90$ km, on mare material. They found 50 craters (5.4%) with $e > 1.2$, 27 craters (2.9%) with $e > 1.3$, and 14 craters (1.5%) with $e > 1.5$, with a maximum $e = 2.23$. In the global database presented here, 21% of craters with $D \geq 10$ km have $e > 1.2$, 8.2% have $e > 1.3$, 1.4% have $e > 1.5$, and 0.066% have $e > 2.0$ (17 craters) with a maximum reliable $e = 2.88 \pm 0.02$ for Schiller crater in the highlands (-51.8°N , -39.8°E , $D_{\text{major}} = 184.4$ km, $D_{\text{minor}} = 65.0$ km; note: two other craters $D \geq 10$ km have $e > 2.88$, but the uncertainties are large and only 39% of each rim was traced, resulting in poor fits). The percentages of elliptical craters in this database are significantly larger than previous reports when the cutoff is $e > 1.2$ and 1.3, but they are comparable for >1.5 . The large fraction of “slightly” elliptical craters is significantly larger than that predicted by hydrocode simulations (e.g., Collins et al., 2011) and laboratory experiments (summarized by Bottke et al., 2000) for pristine primary impacts (to which this database’s study was not limited).

There are five likely and nonmutually exclusive explanations for the discrepancy: (1) Different researchers measure only one chord each for the major and minor axes or, if tracing the rim, different researchers might use different vertex spacing along the crater rims, different numbers of vertex points for each crater rim, different tolerances for how closely rims are traced, and could use biased ellipse fitting algorithms (see the supporting information about ellipse fit algorithms). (2) This database contains a mixture of primary and secondary craters, and secondary craters are more likely to be elliptical due to the lower impact energies involved (McEwen & Bierhaus, 2006, and references therein). If secondary craters were removed in future analysis, the fraction of elliptical craters would likely decrease, as was found for martian craters (unpublished, but using data from Robbins & Hynek, 2012). (3) Similarly, this database has a mixture of craters of all preservation states, and there could be scenarios where craters are elongated along a preferential direction and so would become more elliptical as they evolve with geologic time. (4) Some mechanism of preferential erosion along one axis and incomplete rim traces due to that erosion could combine to artificially yield more elliptical craters. (5) Bottke et al. (2000) just studied the lunar maria, and the lunar highlands have extreme slopes that are more likely to cause craters to form and erode to higher ellipticities; neither laboratory nor numerical simulations take this into account, and the past studies of Bottke et al. (2000) and most work in Herrick et al. (2012) tried to eliminate craters on large slopes.

It is not possible at this time to test the first, second, nor third proposed hypotheses. It is not currently possible to disentangle the two components of the fourth proposed hypothesis, but it can be tested by using the ARC_IMG (denoted as Δ) data (fraction of the rim that could be traced) at an arbitrary cutoff and re-do the analysis. To test

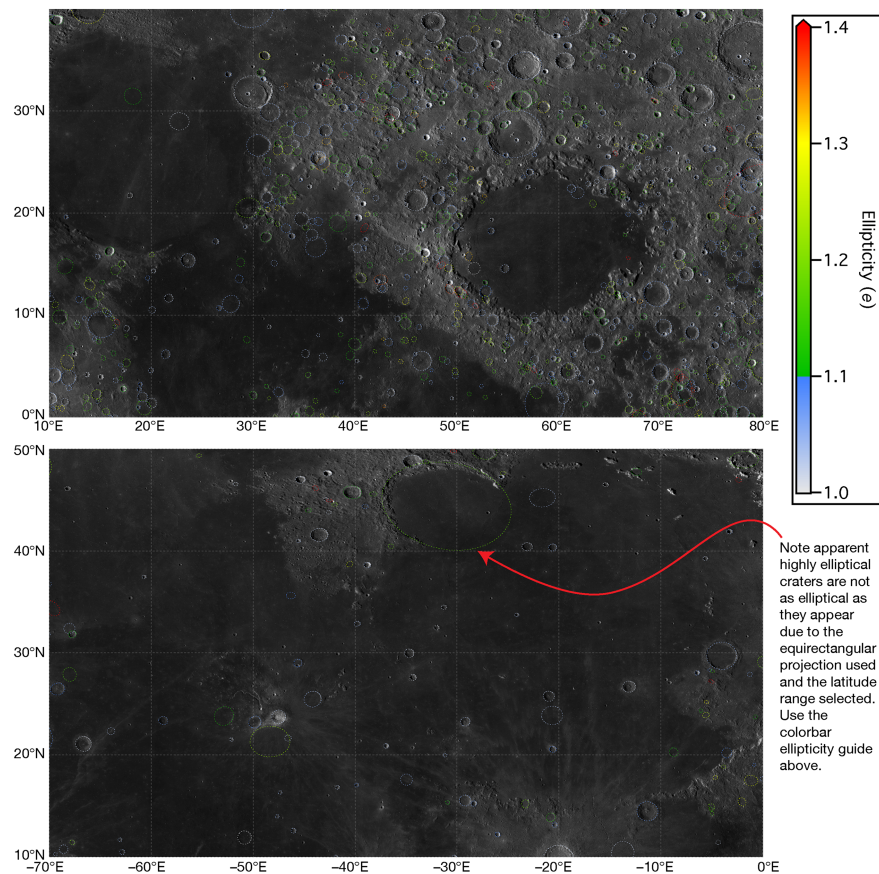


Figure 5. Example regions of the lunar maria showing outlines for all $D \geq 10$ km craters based on best-fit ellipses, color-coded by ellipticity (all $e \geq 1.4$ are red). Outlines of large craters containing the maria have been removed for clarity.

this, $\Delta = 0.65, 0.70$, and 0.75 were used. In that order, $\{14\%, 12\%, 11\%\}$ of $D \geq 10$ km craters have $e > 1.2$, $\{5.0\%, 4.2\%, 3.5\%\}$ of craters have $e > 1.3$, $\{0.76\%, 0.66\%, 0.52\%\}$ of craters have $e > 1.5$, and $\{0.018\%, 0.0070\%, 0.0083\%\}$ of craters have $e > 2.0$. The overall trend is that there are fewer craters of a given ellipticity as one increases the minimum Δ . The change is linear for $e > 1.2, 1.3$, and 1.5 cutoffs between the three Δ values, but the fraction of $e > 2.0$ craters for the three Δ cutoffs is significantly smaller than the other ellipticities relative to no Δ cutoff. This can be interpreted as supporting hypothesis 4 that more incomplete rims, possibly from erosion along a preferred direction, result in more elliptical craters. Unfortunately, larger craters are more likely to have less complete rims due to their overall older age, so removing these craters from a diameter-based analysis could yield artificially biased results (e.g., if Figure 6a were recalculated with this cutoff).

The fifth hypothesis—maria-only craters—can be tested by repeating the original analysis just for craters in lunar maria, as defined by the LROC team's PDS-released map of maria units. Of $D \geq 10$ km craters in the maria, 15% have $e > 1.2$, 5.0% have $e > 1.3$, 1.1% have $e > 1.5$, and the maximum is 1.61 (the largest crater with $e > 2.0$ in the maria is $D = 5.3$ km). This is still larger than the Bottke et al. (2000) results for $e > 1.2$ and > 1.3 . Figure 5 illustrates two large regions of the lunar maria with best-fit ellipses of $D \geq 10$ km craters overlaid and color coded based on e . In these regions, craters that are more elliptical in the maria tend to be buried or have less complete rims, though there are still many large, incomplete craters that also have ellipticities close to 1.0. The supporting information describes why the $D \geq 10$ km cutoff was chosen globally; a similar analysis for just the lunar maria suggests ellipticity values may be reliable for maria craters as small as $D > 2-3$ km. If $D \geq 3$ km is instead used as a threshold, 19% of craters are $e > 1.2$, $8.6\% e > 1.3$, $1.8\% e > 1.5$, and $0.09\% e > 2.0$ (four craters). The reason for larger fractions of elliptical craters is almost certainly due to kilometer-scale secondary craters, such as the vast Copernicus crater secondary field. The SFD_{EDF} analysis of maria craters has lower percentages of $D \lesssim 10$ km craters that are elliptical but otherwise looks similar (similar to Figure 6a, but not shown). From this test, it is clear the maria have a different population of

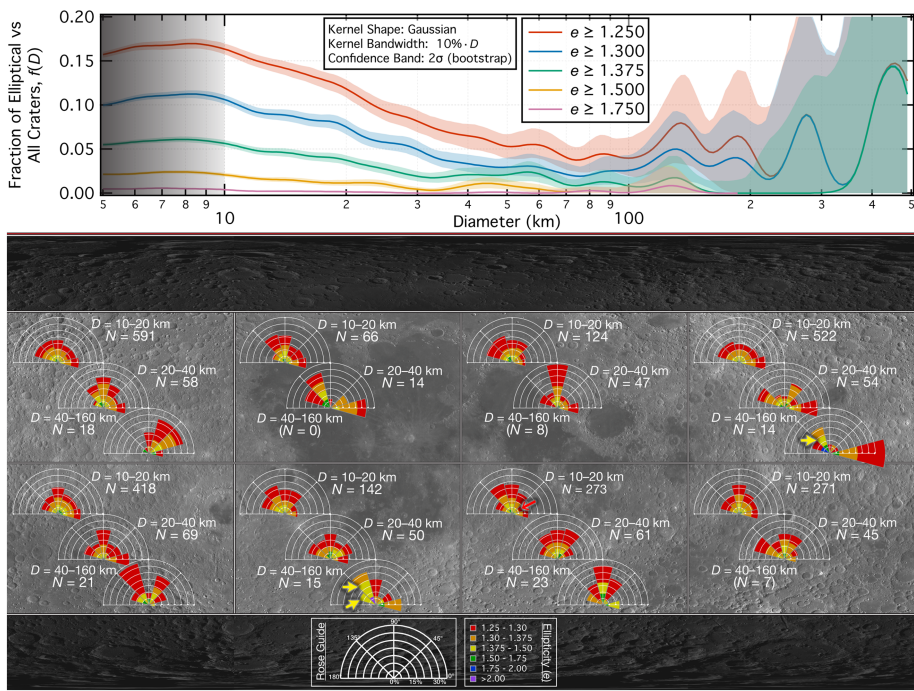


Figure 6. Ellipticity analysis. (top) Relative histograms similar to SFD_{EDF} of crater ellipticities larger than a certain e as a function of diameter; gray gradient over $D < 10$ km indicates region where I do not consider the results reliable. (bottom) Map (background is WAC morphologic) with rose diagrams every $60^\circ \times 90^\circ$ (latitude \times longitude) of craters with ellipticities $e \geq 1.25$. In each region, upper-left plot is craters $D = 10-20$ km, middle is $20-40$ km, lower-right is $40-160$ km; only if >12 craters with $e \geq 1.25$ were present is the plot shown. Colors represent ellipticity ranges, azimuth indicates major axis tilt binned in 30° intervals ($\theta > 165^\circ$ is included in -15° to $+15^\circ$ direction), and magnitude indicates fraction of craters in that diameter and tilt angle ranges where each arc is 5% of the total, and outer radius is 35%. Radial magnitude (percentages) are cumulative with ellipticity, such that if $e \geq 2.0$ is 1% and $e = 1.75-2.0$ is 3%, the latter would span between 1% and 4%. Closed arrows indicate a statistically significant increase in number of craters at the 95% level, and open arrows are a statistically significant decrease. See section 5.1 for discussion.

elliptical craters in this database than the globe, but it is still not entirely possible to directly compare to the Bottke et al. (2000) results because of inclusion of secondary craters.

Both these two tests demonstrate that these factors contribute to higher ellipticity in this database than what has been demonstrated before. The addition of preservation state and secondary versus primary crater classification in future iterations of the database will allow the other hypotheses to be tested and permit more direct comparisons with previously published studies. However, I posit that the analysis in this work is still interesting, for an investigation of the ellipticity of all craters has not been done before, and it can provide a baseline of expectations of elliptical craters across solar system bodies when those craters are not separated into different groups.

A similar analysis is shown in the top panel of Figure 6, which shows the relative fraction of elliptical craters with different ellipticity cutoffs, constructed from ISFD_{EDF} for each ellipticity. This is another way of examining the fraction of elliptical craters as a function of diameter. From those histograms, reading from small to large craters, the fraction of elliptical craters is large for any given ellipticity threshold, the fraction drops until $D \approx 40$ km, and it is relatively stable throughout larger diameters, and this holds throughout the full $D < 2,500$ km range ($D < 500$ km is shown). If the analysis were redone for ARC_IMG ≥ 0.75 (eliminating 14% of all craters, but eliminating disproportionately 51% of all $D \geq 10$ km craters), the overall trend is similar, but there are no craters with $e \geq 1.25$ between approximately 100 and 350 km. This could be interpreted as contrary to predictions of elliptical craters increasing for $D \sim 100$ s km by Collins et al. (2011), but the 2σ uncertainty envelope is too large to distinguish between a steady or increasing fraction.

A separate type of analysis, which appears to not have been published before, is shown in the bottom panel of Figure 6. This panel presents sets of rose diagrams for craters in different regions, and the

craters are further divided into diameter ranges. Within those diameter ranges, the rose diagrams show the percentage of craters with any given tilt angle (in 30° bins) and are color coded based on the fraction of those with a certain ellipticity. The rose diagrams are to test whether the tilt angle of the craters, as both a function of ellipticity and diameter, shows any deviation across the lunar surface from what would be predicted by randomness. A priori, one might expect the highlands (the regions on the far side) to have more elliptical craters than the maria due to the steeper slopes and more substantial erosion.

To determine significance, 100,000 Monte Carlo simulations were carried out for each rose diagram due to different N craters per rose diagram. The simulations sampled crater ellipticities within each diameter range, using bootstrap with replacement from the real database. Tilt angle was randomly sampled from a uniform distribution between 0° and 180°, and any >30° were removed to simulate any given tilt angle range (since the rose diagrams have azimuthal bins of 30°, this simulates just craters in one bin). Crater ellipticities for each simulation were clipped for $e \geq 1.25$, and the fraction that were in each ellipticity bin was stored. Then the median and inner 95th percentile of the fraction of craters from the simulations within each ellipticity bin for that diameter range were calculated. This result was compared with the matching rose diagram. Because there are 126 different values (6 ellipticity ranges and 21 different rose diagrams), these comparison data are not shown.

The null hypothesis is that the craters have random tilts, and that would be rejected if any angle bin, for any diameter, for any ellipticity range, was less than or greater than the inner 95th percent of the simulation. Built into that is the data's own uncertainty based on $N^{1/2}$ Poisson statistics, which cannot be shown in the Figure due to clarity considerations. An example analysis follows: In the $D = 40\text{--}160$ km rose diagram for 0°–90°E by 0°–60°S, there are 23 craters, such that a single crater would be 4.3% of the total. The slice spanning $90 \pm 15^\circ$ has a value and associated uncertainty of $30\% \pm 12\%$ for $e = 1.25\text{--}1.30$, $17\% \pm 9\%$ for $e = 1.30\text{--}1.375$ and $1.375\text{--}1.50$, $9\% \pm 6\%$ for $e = 1.50\text{--}1.75$, and 0% for the two larger e bins. The Monte Carlo simulation for 23 craters for the diameter range 40–160 km has, at 95% confidence, 0–26% of craters $e = 1.25\text{--}1.30$, 0–22% $e = 1.30\text{--}1.375$, 0–13% $e = 1.375\text{--}1.50$, and 0–0% for larger ellipticities. While the value without uncertainty of the data is beyond the range for both smaller ellipticity bands, with their uncertainties, they are within the 95% confidence range, and therefore the null hypothesis is not rejected.

Arrows indicate where the null hypothesis—that the data have random tilts—was rejected because the fraction of craters within the given ellipticity range, tilt angle, and diameter range for that region of the Moon is outside of the inner 95th percentile of the simulation (full arrows are where the observations exceed the simulation, and open is where there is a deficit). In total, only 4 of the 756 different possible ranges are statistically significant (21 rose diagrams, 6 ellipticity ranges, and 6 angle bins combine for 756 points to test). Since that represents only 0.5% of the total, and a 95% confidence band was used, I interpret these results as being consistent with randomness. There is no preferential orientation for 10- to 160-km elliptical craters on the Moon, when divided into these regions.

5.2. Spatial Density

The remainder of this section focuses on different observations that are made using absolute and relative crater spatial density maps, potential explanations for the observations, and/or comparison with past work in that area. Similar trends found from other databases over similar diameter ranges are important to identify because it helps show the reliability of this database. Spatial density maps are shown in Figures 8 and 9 using a 151.5 and 454.5 km (5° and 15°) radius of interest, the latter for compatibility with Povilaitis et al. (2018) and to accommodate fewer large craters. The maps (Figure 8) are for $D \geq 20$ km, $D = 5\text{--}20$ km, and $D = 1.5\text{--}5$ km (5° map masked where Figure 4 shows incomplete data at any diameter $D > 1.5$ km), and the three ratios 1.5/5, 1.5/20, and 5/20 (Figure 9); additional comparisons, and maps relative to the Head+Povilaitis et al. databases, are in the supporting information.

The first several observations are apparent regardless of smoothing radius, and they help show that this database readily reproduces known phenomena. First, the lunar maria and highlands have significantly different crater spatial densities—something that has been known for centuries.

Second, smaller craters overall have a smoother distribution than larger craters, though they still show the maria versus highlands dichotomy. This second observation could be explained by two process: (a) The

kilometer-scale crater population has reaccumulated more quickly than larger craters, both from primary impacts and large fields of secondary craters. (b) Small highlands craters in most areas have reached a steady state population of production and degradation/erasure such that even relatively younger highlands terrain can accumulate the same number of craters as older terrain. This is related to the explanation used earlier in this work to potentially account for “incompleteness” in the highlands for $D \approx 1$ km craters, and it could be tested through a detailed saturation analysis (left to future work). While this observation has been noted for decades, most analyses are based on studies that did not include secondary craters in the population; therefore, that this persists even when including secondary craters is a notable observation.

The third observation is the presence of a large, not generally identified low spatial density region in and around Schrödinger crater (-74.6°N , 132.6°E , $D = 321$ km) that persists across all three diameter ranges. Similar low-density signals from young, large craters are seen throughout the density maps. While this is not surprising and is easily attributed to erasure due to the large crater’s formation, it nonetheless is very obvious in this type of map and is not as apparent in other databases.

Fourth, continuing observations that have been made before (e.g., Head et al., 2010), Orientale crater has unique patterns of spatial density surrounding it, with clear northwest-southeast deficits in crater spatial density that tend to be correlated with large, tens of kilometers secondary crater chains scouring the terrain. This interpretation is supported by the spatial density maps showing that the pattern nearly disappears at the smallest craters examined. It is also supported by the tilt angle of $D \sim 10$ s km craters in the area.

Fifth, the high northern latitudes have a large spatial density of small craters, the highest measured in this data set except in the 5° map near Antoniadi crater. From a literature search, this has not been identified before. I hypothesize it is due to previously unrecognized secondary craters because, dynamically, there is no reason for the lunar north pole to have a marked increase in primary impact events (e.g., Le Feuvre & Wieczorek, 2011). Figure 7a is $\sim 5,000$ km 2 near the lunar north pole, centered on the floor of Byrd crater, and it shows a surface that appears saturated for kilometer-scale impacts, including many with overlapping rims that are typical of secondaries. However, there is no obvious source primary, and so exploring this is left for future work.

The sixth observation is based on the 5° smoothing radius map: The $D = 5\text{--}20$ km crater population shows the most variation in spatial density, spanning 3.5 orders of magnitude, while the $D \geq 20$ km shows the least with approximately 1.5 orders (truncated at the low end due to no craters present). This difference can be explained the same way as the second observation: the degradation/erasure process has a cutoff at a few kilometers at this epoch in lunar history.

Seventh, there are many regions in the 5° map of $D = 1.5\text{--}5$ km craters that have a partial or even full annulus of enhanced crater spatial density. While this is not in and of itself diagnostic of secondary craters, it is highly suggestive, and visual inspection of these regions does, indeed, reveal them to be large secondary crater fields. One such region is around Antoniadi (-69.4°N , 187.0°E , $D = 138$ km), where multikilometer secondaries extend tens of kilometers from the rim and result in the largest spatial densities observed, with over 7,000 craters per 10 6 km 2 , $\sim 2\text{--}7\times$ the average lunar highlands. Antoniadi is shown in Figure 7b along with part of its vast secondary field, apparent by similarly sized, kilometer-scale craters arranged in long chains or tight clusters. Also clear in Figure 8 is Copernicus’ secondary field (9.6°N , -20.1°E , $D = 93$ km) with a spatial density of $D \geq 1.5$ km craters exceeding the average highlands. Aristoteles (50.3°N , 17.3°E , $D = 87$ km) also stands out, as does Humboldt (27.2°S , 81.0°E , $D = 204$ km), and they look similar to Figure 7b. What these results demonstrate is that, at the very least, kilometer-scale secondary craters are present in a myriad of lunar locations, across both dominant terrain types, and potentially cover a nontrivial surface area.

Using the relative maps (Figure 9), additional observations are made. The eighth in this discussion is that there is a significant increase in 5–20 km craters relative to larger craters, centered near the rim of Sinus Iridum (increase centered $\sim 45^\circ\text{N}$, $\sim -35^\circ\text{E}$). This region (Figure 7c) is an island of nonmare material in the maria and contains several superposed and nearby $D \approx 30\text{--}40$ km craters (magenta in Figure 7c) that also have large secondary crater fields. Therefore, multikilometer secondaries (green and blue in Figure 7c) is the plausible explanation. There is a similar increase in 1.5–5 km craters relative to the other ranges near Copernicus and Aristoteles craters in Figure 9, where the latter enhancement travels west, following the maria unit that includes Mare Frigoris. It is likely these are also due to secondary craters.

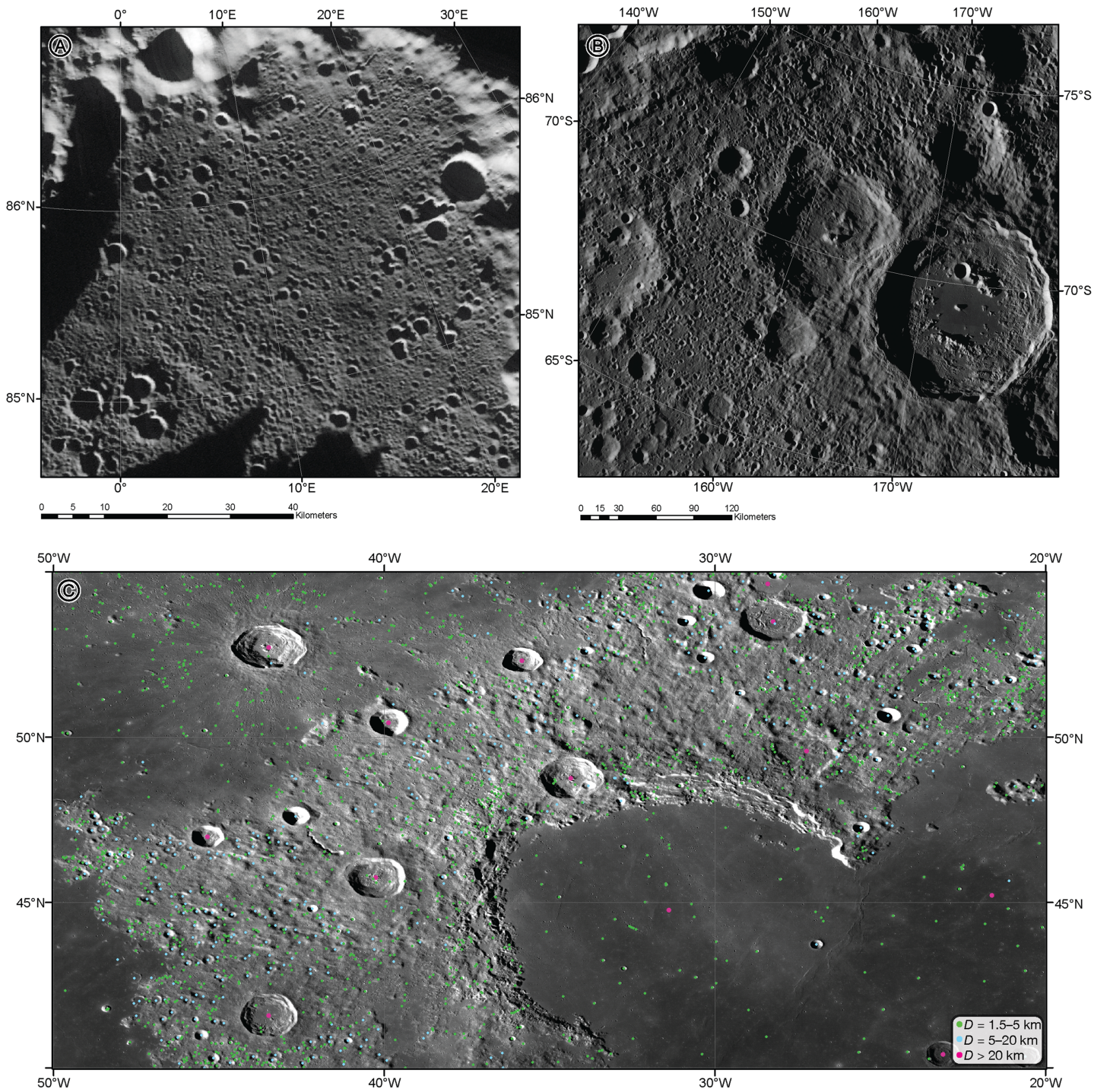


Figure 7. Example regions in support of some observations in section 5.2. In all panels, basemap is the WAC morphologic, but especially relevant to panel (a), craters were also identified in other data sets, including topography. (a) Small region of high northern latitudes, dominated by the floor of Byrd crater. This region shows a large concentration of small, kilometer-scale impact craters and represents a portion of the area described as the largest spatial density of small craters on the Moon. (b) Region of high southern latitudes, dominated by Antoniadi crater and showing the many small craters radiating from it, as an example of enhanced spatial density annuli around large impact craters. (c) Maria region focused on nonmare terrains around Sinus Iridum; this image is in support of observations 8 and 9 in section 5.2.

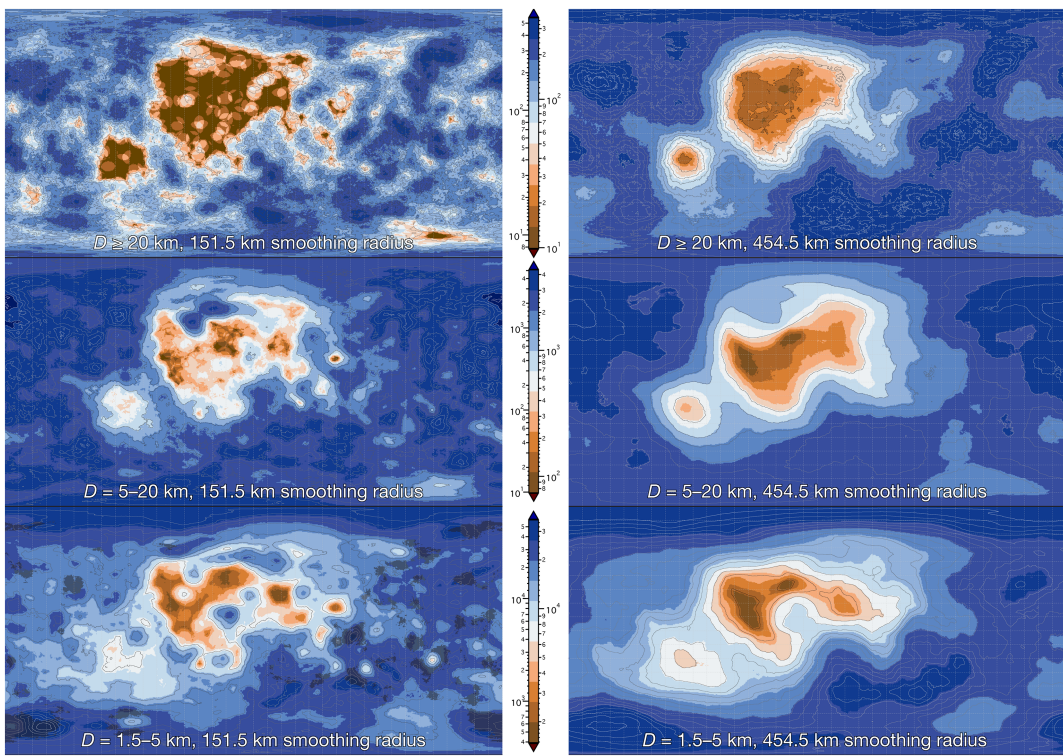


Figure 8. Crater spatial density maps with prime meridian (0°) in the middle, spanning -180° to $+180^\circ$ E by -90° to $+90^\circ$ N (thin grid lines every 10°). All maps were created by examining craters within an x -km radius of each point, where $x = 151.5$ km in the left column (5° at the equator) and 454.5 km (15° at the equator) in the right column. The maps are the spatial density of craters in the labeled diameter ranges, and the scale bars are number of craters per 10^6 km^2 with separate left versus right values for each color. Light contours are overlaid on every plot to aid interpretation. In the 151.5-km-radius maps, some grid points had 0 craters, so these are marked by dark reddish brown. For the 1.5- to 5-km maps, regions where Figure 4 indicated completeness at diameters >1.5 km are shown as gray with contours remaining. See section 5.2 for discussion.

Ninth is that there are areas of significant deficits in both smaller crater ranges relative to $D \geq 20$ km craters. The most significant deficit is north of the *Apollo 17* landing site, on the outcrop of highlands (or southeast rim of Serenitatis). This observation could be explained by the highly reworked nature of the rim leaving both a deficit of large (or identifiable) craters and small craters alike. Significant relative deficits of smaller craters are also present toward the west and north of Orientale. This could be explained by the Orientale-forming impact removing 10s km impacts in the area, the extreme roughness of the terrain making subsequently emplaced craters difficult to identify and rapidly erode, and/or small craters have not had enough time to form in significant numbers. Finally, there is a relative decrease in 1.5- to 5-km craters relative to 5- to 20-km craters northwest of Sinus Iridum, which is opposite to 5- to 20-km versus >20 -km craters discussed above. This could be explained by the large quantity of secondary craters $D > 5$ km (blue in Figure 7c; e.g., Louville A, B, E; Mairan F, Y; Sharp U, B; and Bouguer B), likely from the impact that formed Sinus Iridum, having removed smaller craters in the recent past.

The last observation from these maps (Figures 8 and 9) uses the 454.5-km smoothing radius, which shows there is a deficit of $D \geq 20$ km craters very roughly centered in intensity near Mosoviense crater that continues westward (also observed in Head et al., 2010). This shows as pink in the top and middle relative density plots, indicating the deficit is of large craters, not an enhancement of small craters. I hypothesize it could be attributed to the two basins that are Mosoviense and other nearby hundreds of kilometer craters (e.g., Mendeleev [327 km], d'Alembert [232 km], and Campbell [213 km]) obliterating craters that are up to $D \sim 10$ s km, forming a significant deficit of them. Because this happened in the distant past (evidenced by the overprinting and degradation of these large impacts), craters have reaccumulated up to more typical highlands spatial densities, but only for craters $D \lesssim 20$ km (observational constraint based on the Figure, and plausible given that smaller craters form more frequently). Thus, a deficit of $20 \lesssim D \lesssim 10$ s km craters remains, while smaller craters are not enhanced. This is supported by the signal barely showing in the shorter smoothing radius maps, which indicates it is a subtler, broader-scale signal,

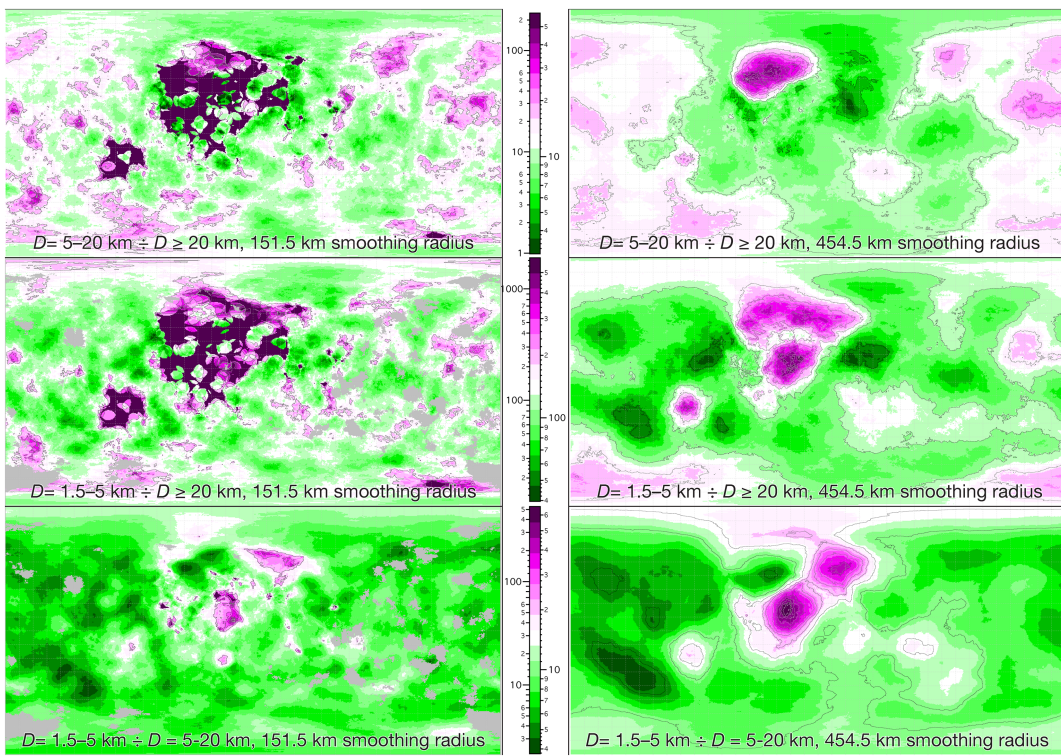


Figure 9. Same as Figure 8, but relative spatial density. The three maps result from combinations of the Figure 8 plots divided by each other to show the ratio of craters in different diameter ranges.

which is more typical of older events. As this was the only area also studied by Povilaitis et al. (2018), it must be noted that my interpretation is different. They observed an excess of $D = 8\text{--}22$ km in the region and interpret the excess as an increase in multikilometer secondaries from hundreds of kilometer craters (as opposed to a decrease of tens of kilometer craters). They stated that the obliteration of $D \gtrsim 20$ km craters would “make little sense” because it would eliminate small craters. However, this database shows only a slight enhancement in $D = 5\text{--}20$ km craters in the region and it is not centered on Moscoviene. Also, based on Figures 2 and 3, and S5–S6, it is likely that the Head + Povilaitis et al. databases missed craters that could alter their conclusions.

6. Summary and Future Work

This paper presented a new impact crater database of lunar craters that numbers over 2 million, with 1.3 million having diameters $D \geq 1$ km. Based on an analysis of the SFD of the craters across the lunar surface (Figure 4), it is estimated to be a complete census of all craters $D \geq 1\text{--}2$ km. The database has many more craters $D \lesssim 20\text{--}30$ km than other existing databases (Figure 2), which I attribute to using multiple data sources for crater identification, this being a fully manual effort rather than automated, and having a more liberal philosophy about cataloging features which could be impact craters. For the craters that do overlap in the different catalogs, this database compares well (Figure 1).

Two main sets of observations were made with the database in section 5 to demonstrate similarities with some past work and show new trends (or lack thereof) using the data afforded by a database of this type. In the ellipticity analysis, many more elliptical craters were identified in this database than in past efforts, likely because this database does not yet discriminate based on primaries versus secondaries, preservation state, and local terrain slope. A unique ellipticity analysis was done to test whether the tilt angles of craters $D \geq 10$ km showed any preference for direction, and the null hypothesis that they do not was not rejected. The spatial density analysis yielded several different observations, many of them made in previous work, but important nonetheless to show reliability for this database or to hypothesize about where and why differences are present.

Significant future work could be done with this database, not only in scientific investigations from it, but expanding the database itself. I am currently in the process of adding morphology and morphometry measurements, which should expand its utility. The morphology data includes (a) confidence the features are impact craters, (b) identifies features common to secondary craters, and (c) lists common simple and complex crater characteristics. The morphometry data includes (d) crater depths calculated from WAC DTMs, LOLA RDR, and the merged *SELENE* DTM + LOLA product. The grant that supports this additional work includes validation of a small percentage of the craters to better understand the uncertainties based on how different researchers interpret the data.

In conclusion, this database of 1.3 million impact craters $D \geq 1\text{--}2$ km is being provided to the scientific community as a product that can assist future studies. While it is a complete product, using the database properly requires knowledge of and accounting for caveats described throughout this text. In particular, careful attention to the formal uncertainties, caveats with respect to minimum diameters for reliable ellipse parameters, and consideration of the fraction of the rim that was traced in combination with the vertex points used are all recommended. As with any database, researchers should verify that it is appropriate for their needs. Additionally, it will be superseded in a few years, upon the completion of the expansion described in the previous paragraph. Interested individuals are encouraged to contact me for more information, including updates, and $D \leq 1$ km craters.

Appendix A

This crater database contains 21 columns of data for each crater that are described in brief here. The suffix “_IMG” is used because these data were derived using imagery or topography as imagery, and future work will include parameters derived from other sources such as DTMs and laser shot data.

CRATER_ID	Catalog identifier string in the format ##-#-#####. The first two numbers are the WAC region in which the crater was identified based on the 10 global WAC tiles. The third number corresponds to the data source used to identify the feature (section 3.3), and the last six digits are the order in which the crater was identified. Note: These IDs might change in future versions of the catalog, but the format will remain the same.
LAT_CIRC_IMG	North latitude in decimal degrees from a circle fit.
LON_CIRC_IMG	Positive East longitude in decimal degrees from a circle fit, in the -180° to $+180^\circ$ domain.
LAT_ELLI_IMG	North latitude in decimal degrees from an ellipse fit.
LON_ELLI_IMG	Positive East longitude in decimal degrees from an ellipse fit, in -180° to $+180^\circ$ domain.
DIAM_CIRC_IMG	Diameter in kilometers from a circle fit.
DIAM_CIRC_SD_IMG	Standard deviation of kilometers of the fit residuals. Each manual rim point’s distance from the crater center was calculated and subtracted from the best-fit radius, and this value is the standard deviation of those differences.
DIAM_ELLI_MAJOR_IMG	Major axis in kilometers from an ellipse fit.
DIAM_ELLI_MINOR_IMG	Minor axis in kilometers from an ellipse fit.
DIAM_ELLI_ECCEN_IMG	Eccentricity (unitless) of the ellipse, calculated as $(1 - b^2 \div a^2)^{1/2}$ where a is the major and b the minor axes.
DIAM_ELLI_ELLIP_IMG	Ellipticity (unitless) of the ellipse, calculated as $a \div b$.
DIAM_ELLI_ANGLE_IMG	Angle of the fitted ellipse in degrees, counter-clockwise from the major axis oriented East-West.
LAT_ELLI_SD_IMG	Formal standard error in the ellipse fit’s center latitude, in degrees.
LON_ELLI_SD_IMG	Formal standard error in the ellipse fit’s center longitude, in degrees.
DIAM_ELLI_MAJOR_SD_IMG	Formal standard error in the ellipse fit’s major axis, in kilometers.
DIAM_ELLI_MINOR_SD_IMG	Formal standard error in the ellipse fit’s minor axis, in kilometers.

DIAM_ELLI_ECCEN_SD_IMG

Formal standard error in the ellipse fit's eccentricity (unitless).
Uses the method of adding in quadrature, defined as

$$\Delta e = \sqrt{\left(\frac{b^2}{a^3} \frac{1}{\sqrt{1-b^2/a^2}} \Delta a\right)^2 + \left(\frac{-b^2}{a} \frac{1}{\sqrt{1-b^2/a^2}} \Delta b\right)^2}$$

DIAM_ELLI_ELLIP_SD_IMG

Formal standard error in the ellipse fit's ellipticity (unitless).
Uses the method of adding in quadrature, defined as

$$\Delta e = \sqrt{\left(\frac{1}{b} \Delta a\right)^2 + \left(\frac{-a}{b^2} \Delta b\right)^2}$$

DIAM_ELLI_ANGLE_SD_IMG
ARC_IMG

Formal standard error in the ellipse fit's tilt angle, in degrees.
An estimation of the fraction of the complete rim that was traced.
See section 3.5 for more detail.

PTS_RIM_IMG

Number of manual points used to identify the crater rim and
calculate the circle and ellipse fits.

Acknowledgments

C. R. Chapman provided presubmission input that benefitted this work. This paper benefited from reviews by R. R. Herrick and G. G. Michael, and review and editorial handling by C. I. Fassett. Support in constructing this database was made possible through the Maryland Space Grant, NASA SSERVI "ISET" award NNH13ZDA006C, Lunar Reconnaissance Orbiter LAMP instrument funds, and NASA SSW award NNX15AH97G. All data that were used to construct the database were freely available through public space agency archives. The database itself is available through the NASA PDS, https://astrogeology.usgs.gov/search/map/Moon/Research/Craters/RobbinsCraterDatabase_20180815.

References

- Al-Sharadqah, A., & Chernov, N. (2009). Error analysis for circle fitting algorithms. *Electronic Journal of Statistics*, 3(0), 886–911. <https://doi.org/10.1214/09-EJS419>
- Arthur, D. W. G., Agnieray, A. P., Horvath, R. A., Wood, C. A., & Chapman, C. R. (1964). The system of lunar craters, quadrant I. *Communications of the Lunar and Planetary Laboratory*, 2, 1.
- Arthur, D. W. G., Agnieray, A. P., Horvath, R. A., Wood, C. A., & Chapman, C. R. (1965). The system of lunar craters, quadrant II. *Communications of the Lunar and Planetary Laboratory*, 3, 1.
- Arthur, D. W. G., Agnieray, A. P., Pellicori, R. H., Wood, C. A., & Weller, T. (1965). The system of lunar craters, quadrant III. *Communications of the Lunar and Planetary Laboratory*, 3, 1.
- Arthur, D. W. G., Pellicori, R. H., & Wood, C. A. (1966). The system of lunar craters, quadrant IV. *Communications of the Lunar and Planetary Laboratory*, 5, 1.
- Baldwin, R. B. (1949). *The face of the Moon*. Chicago, IL: University of Chicago Press.
- Barker, M. K., Mazarico, E., Neumann, G. A., Zuber, M. T., Haruyama, J., & Smith, D. E. (2016). A new lunar digital elevation model from the Lunar Orbiter Laser Altimeter and SELENE Terrain Camera. *Icarus*, 273(C), 346–355. <https://doi.org/10.1016/j.icarus.2015.07.039>
- Barlow, N. G. (2017). Status report on crater databases for Mercury, the Moon, Mars, and Ganymede. Paper presented at the 3rd Planetary Data Workshop, Flagstaff, AZ.
- Barlow, N. G., Mest, S. C., Gibbs, V. B., & Kinser, R. M. (2012). Compilation of a global GIS crater database for the Moon. Paper presented at the 44th Division of Planetary Science of the American Astronomical Society, Reno, NV.
- Blagg, M. A., Müller, K., Wesley, W. H., Saunder, S. A., & Franz, J. (1935). *Named lunar formations*. London, England: P. Lund, Humphries, & Co.
- Bottke, W. F. Jr., Love, S. G., Tytell, D., & Glotch, T. D. (2000). Interpreting the elliptical crater populations on Mars, Venus, and the Moon. *Icarus*, 145(1), 108–121. <https://doi.org/10.1006/icar.1999.6323>
- Collins, G. S., Elbeshausen, D., Davison, T. M., Robbins, S. J., & Hynek, B. M. (2011). The size-frequency distribution of elliptical impact craters. *Earth and Planetary Science Letters*, 310(1–2), 1–8. <https://doi.org/10.1016/j.epsl.2011.07.023>
- Ester, M., Kriegel, H.-P., Sander, J., & Xu, X. (1996). A density-based algorithm for discovering clusters in large spatial databases with noise (Vol. 2, pp. 226–231). Presented at the Proceedings of the Second International Conference on Knowledge Discovery and Data Mining KDD.
- Fassett, C. I., & Thomson, B. J. (2014). Crater degradation on the lunar maria: Topographic diffusion and the rate of erosion on the Moon. *Journal of Geophysical Research: Planets*, 119, 2255–2271. <https://doi.org/10.1002/2014JE004698>
- Fitzgibbon, A., Pilu, M., & Fisher, R. B. (1999). Direct least square fitting of ellipses. *IEEE Transactions on Pattern Analysis and Machine Intelligence*, 21(5), 476–480. <https://doi.org/10.1109/34.765658>
- Galilei, G. (1610). *Sidereus nuncius*. Florence, Italy: self-published by Galileo Galilei. <https://doi.org/10.3931/e-rara-695>
- Hartmann, W. K. (1965). Secular changes in meteoritic flux through the history of the solar system. *Icarus*, 4(2), 207–213. [https://doi.org/10.1016/0019-1035\(65\)90062-X](https://doi.org/10.1016/0019-1035(65)90062-X)
- Hartmann, W. K. (1999). Martian cratering VI: Crater count isochrons and evidence for recent volcanism from Mars Global Surveyor. *Meteoritics & Planetary Science*, 34(2), 167–177. <https://doi.org/10.1111/j.1945-5100.1999.tb01743.x>
- Haruyama, J., Hara, S., Hioki, K., Iwasaki, A., Morota, T., Ohtake, M., Matsunaga, T., et al. (2012). Lunar global digital terrain model dataset produced from SELENE (Kaguya) Terrain Camera stereo observations. Abstract 1659. Paper presented at the 43rd Lunar and Planetary Science Conference, The Woodlands, TX.

- Head, J. W. III, Fassett, C. I., Kadish, S. J., Smith, D. E., Zuber, M. T., Neumann, G. A., & Mazarico, E. (2010). Global distribution of large lunar craters: Implications for resurfacing and impactor populations. *Science*, 329(5998), 1504–1507. <https://doi.org/10.1126/science.1195050>
- Herrick, R. R., Schenk, P. M., & Robbins, S. J. (2012). Surveys of elliptical crater populations on the Saturnian satellites, Mercury, and Mars. *Icarus*, 220(2), 297–304. <https://doi.org/10.1016/j.icarus.2012.05.027>
- Le Feuvre, M., & Wieczorek, M. A. (2011). Nonuniform cratering of the Moon and a revised crater chronology of the inner solar system. *Icarus*, 214(1), 1–20. <https://doi.org/10.1016/j.icarus.2011.03.010>
- Losiak, A., Wilhelms, D. E., Byrn, C. J., Thaisen, K., Weider, S. Z., Kohout, T., O'Sullivan, K., et al. (2009). A new lunar crater database. Abstract #1532. Paper presented at the 40th Lunar and Planetary Science Conference, Houston, TX.
- McEwen, A. S., & Bierhaus, E. B. (2006). The importance of secondary cratering to age constraints on planetary surfaces. *Annual Review of Earth and Planetary Sciences*, 34(1), 535–567. <https://doi.org/10.1146/annurev.earth.34.031405.125018>
- Neukum G. (1983). Meteoritenbombardement und Datierung planetarer Oberflächen (German original). Meteorite bombardment and dating of planetary surfaces (English translation, 1984) (186 pp.). Habilitation Thesis for Faculty Membership, University of Munich.
- Neukum, G., Ivanov, B. A., & Hartmann, W. K. (2001). Cratering records in the inner solar system in relation to the lunar reference system. *Space Science Reviews*, 96(1/4), 55–86. <https://doi.org/10.1023/A:1011989004263>
- Neukum, G., König, B., & Arkani-Hamed, J. (1975). A study of lunar impact crater size-distributions. *The Moon*, 12(2), 201–229. <https://doi.org/10.1007/BF00577878>
- Neumann, G. A., Zuber, M. T., Wieczorek, M. A., Head, J. W., Baker, D. M. H., Solomon, S. C., Smith, D. E., et al. (2015). Lunar impact basins revealed by gravity recovery and interior laboratory measurements. *Science Advances*, 1(9), 10. <https://doi.org/10.1126/sciadv.1500852>
- Öhman, T. (2015). *LPI crater database*. Houston, TX: Lunar & Planetary Institute.
- Povlaitis, R. Z., Robinson, M. S., van der Bogert, C. H., Hiesinger, H., Meyer, H. M., & Ostrach, L. R. (2018). Crater density differences: Exploring regional resurfacing, secondary crater populations, and crater saturation equilibrium on the moon. *Planetary and Space Science*, 162, 41–51. <https://doi.org/10.1016/j.pss.2017.05.006>
- Riccioli, G. B. (1651). *Almagestum novum astronomiam veterem novamque complectens observationibus aliorum* (Vol. 4). Bononiae: ex typographia haeredis Victorij Benatij. <https://doi.org/10.3931/e-rara-520>
- Robbins, S. J., Antonenko, I., Kirchoff, M. R., Fassett, C. I., Herrick, R. R., Singer, K., et al. (2014). The variability of crater identification among expert and community crater analysts. *Icarus*, 234(C), 109–131. <https://doi.org/10.1016/j.icarus.2014.02.022>
- Robbins, S. J., & Hynek, B. M. (2012). A new global database of Mars impact craters ≥ 1 km: 1. Database creation, properties, and parameters. *Journal of Geophysical Research*, 117, E05004. <https://doi.org/10.1029/2011JE003966>
- Robbins, S. J., Riggs, J. D., Weaver, B. P., Bierhaus, E. B., Chapman, C. R., Kirchoff, M. R., et al. (2018). Revised recommended methods for analyzing crater size-frequency distributions. *Meteoritics & Planetary Science*, 53(4), 891–931. <https://doi.org/10.1111/maps.12990>
- Robinson, M. S., Brylow, S. M., Tschimmel, M., Humm, D., Lawrence, S. J., Thomas, P. C., et al. (2010). Lunar Reconnaissance Orbiter Camera (LROC) instrument overview. *Space Science Reviews*, 150(1–4), 81–124. <https://doi.org/10.1007/s11214-010-9634-2>
- Rodionova, J. F., Karlov, A. A., Skobeleva, T. P., Konotopskaya, E. V., Shevchenko, V. V., Kozubskiy, K. E., et al. (1987). In V. V. Shevchenko (Ed.), *Morphological catalogue of the craters of the moon* (p. 174). Moscow: Mosk Gos Univ Press.
- Salamunićar, G., Lončarić, S., Grumpe, A., & Wöhler, C. (2014). Hybrid method for crater detection based on topography reconstruction from optical images and the new LU78287GT catalogue of lunar impact craters. *Advances in Space Research*, 53(12), 1783–1797. <https://doi.org/10.1016/j.asr.2013.06.024>
- Salamunićar, G., Lončarić, S., & Mazarico, E. (2012). LU60645GT and MA132843GT catalogues of lunar and Martian impact craters developed using a crater shape-based interpolation crater detection algorithm for topography data. *Planetary and Space Science*, 60(1), 236–247. <https://doi.org/10.1016/j.pss.2011.09.003>
- Shoemaker, E. M., Hait, M. H., Swann, G. A., Schleicher, D. L., Dahlem, D. H., Schaber, G. G., & Sutton, R. L. (1970). Lunar regolith at Tranquillity Base. *Science*, 167(3918), 452–455. <https://doi.org/10.1126/science.167.3918.452>
- Smith, D. E., Zuber, M. T., Jackson, G. B., Cavanaugh, J. F., Neumann, G. A., Riris, H., et al. (2009). The Lunar Orbiter Laser Altimeter Investigation on the Lunar Reconnaissance Orbiter Mission. *Space Science Reviews*, 150(1–4), 209–241. <https://doi.org/10.1007/s11214-009-9512-y>
- Smith, D. E., Zuber, M. T., Neumann, G. A., Mazarico, E., Lemoine, F. G., Head, J. W. III, et al. (2017). Summary of the results from the lunar orbiter laser altimeter after seven years in lunar orbit. *Icarus*, 283(C), 70–91. <https://doi.org/10.1016/j.icarus.2016.06.006>
- Strom, R. G., Malhotra, R., Xiao, Z.-Y., Ito, T., Yoshida, F., & Ostrach, L. R. (2015). The inner solar system cratering record and evolution of impactor populations. *Research in Astronomy and Astrophysics*, 15(3), 407–434. <https://doi.org/10.1088/1674-4527/15/3/009>
- Szpak, Z. L., Chojnacki, W., & van den Hengel, A. (2015). Guaranteed ellipse fitting with a confidence region and an uncertainty measure for centre, axes, and orientation. *Journal of Mathematical Imaging and Vision*, 52(2), 173–199. <https://doi.org/10.1007/s10851-014-0536-x>
- Taubin, G. (1991). Estimation of planar curves, surfaces, and nonplanar space curves defined by implicit equations with applications to edge and range image segmentation. *IEEE Transactions on Pattern Analysis and Machine Intelligence*, 13(11), 1115–1138. <https://doi.org/10.1109/34.103273>
- Vincenty, T. (1975). Direct and inverse solutions of geodesics on the ellipsoid with application of nested equations. *Survey Review*, XXIII(176), 88–93.
- Wang, J., Cheng, W., & Zhou, C. (2015). A Chang'E-1 global catalog of lunar impact craters. *Planetary and Space Science*, 112(C), 42–45. <https://doi.org/10.1016/j.pss.2015.04.012>
- Wood, C. A., & Andersson, L. (1978). New morphometric data for fresh lunar craters (Vol. 9, pp. 3669–3689). Presented at the Proceedings of the Lunar and Planetary Science Conference.
- York, D., Evensen, N. M., Martínez, M. L., & De Basabe Delgado, J. (2004). Unified equations for the slope, intercept, and standard errors of the best straight line. *American Journal of Physics*, 72(3), 367–375. <https://doi.org/10.1119/1.1632486>
- Young, J. (1953). A catalogue of lunar craters, published privately by D. W. G. Arthur.